Available online at www.sciencedirect.com
ScienceDirect
Cement & Concrete Composites 28 (2006) 959–968
Cement & Concrete Composites
www.elsevier.com/locate/cemconcomp

Cyclic modeling of FRP-confined concrete with improved ductility

Y. Shao [a], Z. Zhu [b], A. Mirmiran [b,*]

[a] Dunn Savoie, Inc., 908 South Cleveland Street, Oceanside, CA 92054, USA
[b] Florida International University, Department of Civil and Environmental Engineering, Miami, FL 33174, USA

Available online 1 September 2006

Abstract

Confinement by fiber reinforced polymer (FRP) wraps can significantly enhance strength and ductility of concrete columns. Behavior of FRP-confined concrete in uniaxial compression can be characterized by its bilinear stress–strain and unique dilation properties. A number of models have in recent years been developed to capture these characteristics under monotonic loading. None, however, have addressed the cyclic response of FRP-confined concrete. A total of 24 FRP-confined concrete stub specimens were tested in uniaxial compression under different levels of loading and unloading, with different fiber type, wrap thickness, and loading patterns. Based on a regression analysis of test results, a constitutive model is developed that includes cyclic rules for loading and unloading, plastic strains, and stiffness and strength degradations. The proposed model is validated by comparing analytical predictions with experimental results of an independent test series. Good agreement was shown between the analysis and experiments, confirming the ability of the model to predict the cyclic behavior of FRP-confined concrete. The model could be easily implemented in a fiber element model for flexural analysis of cyclic loaded beam-columns in conjunction with a strain gradient approach.

Keywords: Concrete; Confinement; Constitutive modeling; Cyclic loading; Ductility; FRP

1. Introduction

Confinement by fiber reinforced polymer (FRP) wraps can significantly enhance strength and ductility of concrete columns. In the last decade, fiber-wrapping has been successfully applied as a viable retrofitting measure for existing concrete columns. Loud [1] reported that fiber-wrapped columns withstood the 1994 Northridge earthquake with no damage. Behavior of FRP-confined concrete in compression can be characterized by its bilinear stress–strain and unique dilation properties. Samaan et al. [2] proposed a bilinear model to trace the entire stress–strain curve for FRP-confined concrete in monotonic compression. The model correlated the dilation rate of concrete with the hoop stiffness of the FRP. In recent years, other confinement models have also been developed [3,4]. A comprehensive review of the performance of available models for FRP-confined concrete has been reported by several researchers [5–7]. None of the available models, however, have addressed the cyclic response of FRP-confined concrete.

The present study provides a computer model based on a solid experimental database for cyclic loading and unloading of FRP-confined concrete in uniaxial compression. Using the existing modeling approaches for unconfined concrete and steel-confined concrete [8–10], a constitutive model is developed that includes cyclic rules for loading and unloading, plastic strains, and stiffness and strength degradations.

2. Experimental work

2.1. Specimen preparation and test procedure

A total of 24 FRP-wrapped concrete stubs were tested under cycles of loading and unloading in uniaxial

* Corresponding author. Fax: +1 305 348 2314.
E-mail address: mirmiran@fiu.edu (A. Mirmiran).

0958-9465/$ - see front matter © 2006 Elsevier Ltd. All rights reserved.
doi:10.1016/j.cemconcomp.2006.07.009

Table 1
Mechanical properties of FRP wraps

Type	Glass fibers (SikaWrap Hex 100G)	Carbon fibers (SikaWrap Hex 103C)	Epoxy resin (Sikadur Hex 300)	GFRP laminate (Glass + Epoxy)	CFRP laminate (Carbon + Epoxy)
Tensile strength (MPa)	2275	3790	72.5	610	850
Tensile modulus (MPa)	72,400	234,430	3165	26,130	70,605
Maximum elongation (%)	4.0	1.5	4.8	2.5	1.1

compression. The stubs were 152 mm in diameter and 305 mm in height, and were all made of the same batch of concrete with a 28-day compressive strength of 40 MPa. Both glass and carbon FRP wraps were used. Table 1 shows the mechanical properties of the epoxy saturated FRP wraps and each individual component. The unidirectional fibers were wrapped only in the hoop direction of the concrete cylinder. The wrapped specimens were labeled with C or G for carbon or glass, respectively, 1 or 2 for number of layers of the wrap, and 1–6 for the loading patterns. Table 2 shows the test matrix and the loading patterns. Three cycles of loading and unloading were carried out as listed in the table. Axial shortening was monitored using two linear variable differential transducers (LVDT). Four strain gages were attached at the mid-height of each specimen, two in the axial direction, and two in the hoop direction.

Table 2
Test matrix and loading patterns

Type of FRP	Number of layers	Specimen name	Steps in loading pattern		
			Step 1 (%)	Step 2 (%)	Step 3 (%)
Glass Wrap	1	G11	0–100[a]	–	–
		G12	0–40 (3)[b]	0–100	–
		G13	0–60 (3)[b]	0–100	–
		G14	0–80 (3)[b]	0–100	–
		G15	0–80	40–80 (3)[b]	40–100
		G16	0–80	60– (3)[b]	60–100
	2	G21	0–100	–	–
		G22	0–40 (3)[b]	0–100	–
		G23	0–60 (3)[b]	0–100	–
		G24	0–80 (3)[b]	0–100	–
		G25	0–80	40–80 (3)[b]	40–100
		G26	0–80	60–80 (3)[b]	60–100
Carbon wrap	1	C11	0–100	–	–
		C12	0–40 (3)[b]	0–100	–
		C13	0–60 (3)[b]	0–100	–
		C14	0–80 (3)[b]	0–100	–
		C15	0–80	40–80 (3)[b]	40–100
		C16	0–80	60–80 (3)[b]	60–100
	2	C21	0–100	–	–
		C22	0–40 (3)[b]	0–100	–
		C23	0–60 (3)[b]	0–100	–
		C24	0–80 (3)[b]	0–100	–
		C25	0–80	40–80 (3)[b]	40–100
		C26	0–80	60–80 (3)[b]	60–100

[a] Percentages represent fractions of the monotonic capacity.
[b] Three cycles of loading and unloading at the percentages listed.

2.2. Test results and observations

Fig. 1 shows the typical failure modes. Failure was in the form of fiber rupture in the hoop direction, generally sudden with no advance warning. There was no apparent difference between the failure modes of the cylinders with one or two layer wraps. In general, rupture of the GFRP wraps appeared to be more contained within the mid-height of the specimens, whereas the CFRP wraps basically unzipped throughout the entire height of the specimens.

Table 3 shows confinement ratio and confinement effectiveness for the specimens. In the same table, test data from three sources [11–13] are shown for comparison. As will be discussed later, the first two series of tests were used for calibration of the model, while the latter was used only for verification of the model through blind prediction.

Confinement effectiveness is defined as the ratio of confined strength f'_{cu} to unconfined strength f'_{co} of concrete. Confinement effectiveness is generally considered to be a function of confinement ratio, CR, as given by:

$$\mathrm{CR} = \frac{f_r}{f'_{co}} \tag{1}$$

where f_r is the confining pressure from FRP, as

$$f_r = \frac{2 f_j t_j}{D} \tag{2}$$

where f_j is the tensile strength of the wrap, t_j is the thickness of the wrap, and D is diameter of concrete core. It appears that for ratios below a threshold of 0.3, confinement is not fully effective, and the wrap only contributes to ductility rather than strength of concrete core.

Fig. 2 shows plots of axial stress versus axial and hoop strains for all specimens in the same scale. The initial slope of the curves is the same as that of concrete core, since the fibers are only in the hoop direction. The response curve becomes softer as concrete begins to dilate further. The bend point in the response is about 70% of the ultimate strength. Single layer of GFRP or CFRP does not provide any strength enhancement for concrete, while an increased ductility is observed. The ultimate strains for the GFRP stubs are higher than those of their CFRP counterparts with the same number of layers. Therefore, confinement with GFRP provides better ductility for concrete. On the

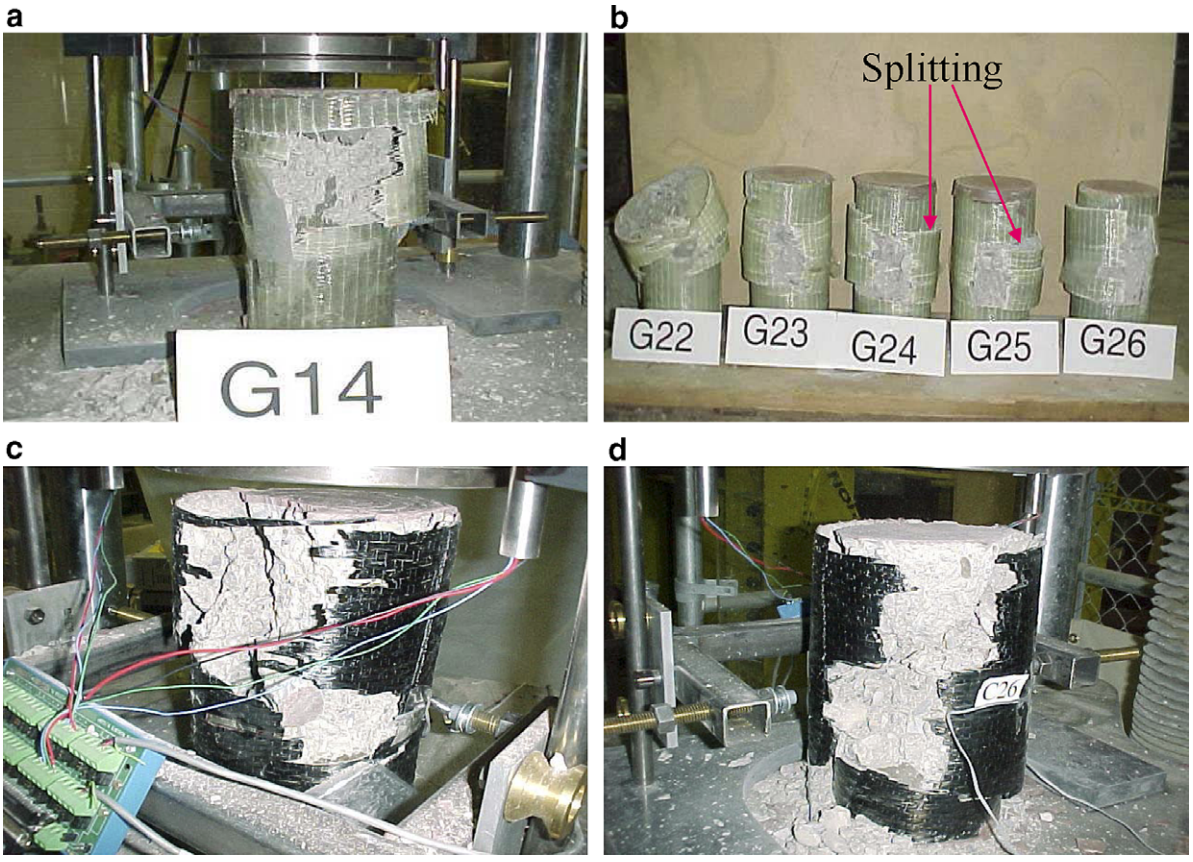

Fig. 1. Typical failure modes: (a) single layer glass warp; (b) two-layer glass warps; (c) single layer carbon warp; (d) two-layer carbon warp.

Table 3
Confinement ratio and confinement effectiveness for FRP-wrapped concrete stubs

	Series	f''_{co} (MPa)	f_j (MPa)	t_j (mm)	CR	f''_{cu} (MPa)	f''_{cu}/f''_{co}
Present study[a]	Single layer E-glass wrap	40.2	610	1.02	0.20	49.6	1.23
	Two layer E-glass wrap			2.03	0.41	71.4	1.78
	Single layer carbon wrap		850	1.02	0.28	59.4	1.48
	Two layer carbon wrap			2.03	0.56	91.8	2.28
Scherer (1996)[a]	14 layer E-glass tube	30.9	641	2.97	0.81	86.2	2.79
Mastrapa (1997)[a]	Seven layer S-glass bonded wrap	37.2	586	4.06	0.84	111	2.98
	Seven layer S-glass unbonded wrap					112	3.01
	Seven layer S-glass unbonded wrap					110	2.96
Chen (2001)[b]	Two layer carbon wrap	39.6	3550	0.33	0.39	95.0	2.40
	Three layer carbon wrap			0.50	0.60	112.36	2.84

[a] Used for calibration of the proposed model.
[b] Used for validation of the proposed model.

other hand, ultimate strengths of CFRP specimens are higher than those of GFRP specimens. The differences in strength and ductility may be attributed to the difference in the tensile strength and modulus for the CFRP and GFRP wraps.

Cyclic response of FRP-confined concrete depends on the level of unloading, and whether it occurs prior to or after the bend point in the envelope curve. The unloading curve can be characterized as linear elastic, when unloading starts below the bend point (Fig. 3a). On the other hand, when concrete is loaded beyond the bend point, its unloading curve is clearly nonlinear with a distinct plastic or residual strain (Fig. 3b). The shape of the reloading curve is almost always linear. The reloading curve does not return to the original unloading stress, but rather a lower stress level, with distinct strength degradation and much energy dissipation (Fig. 3c). However, when reloading initiates just below the unloading point, the curve almost fully returns to the unloading stress, with negligible strength degradation and little energy dissipation (Fig. 3d).

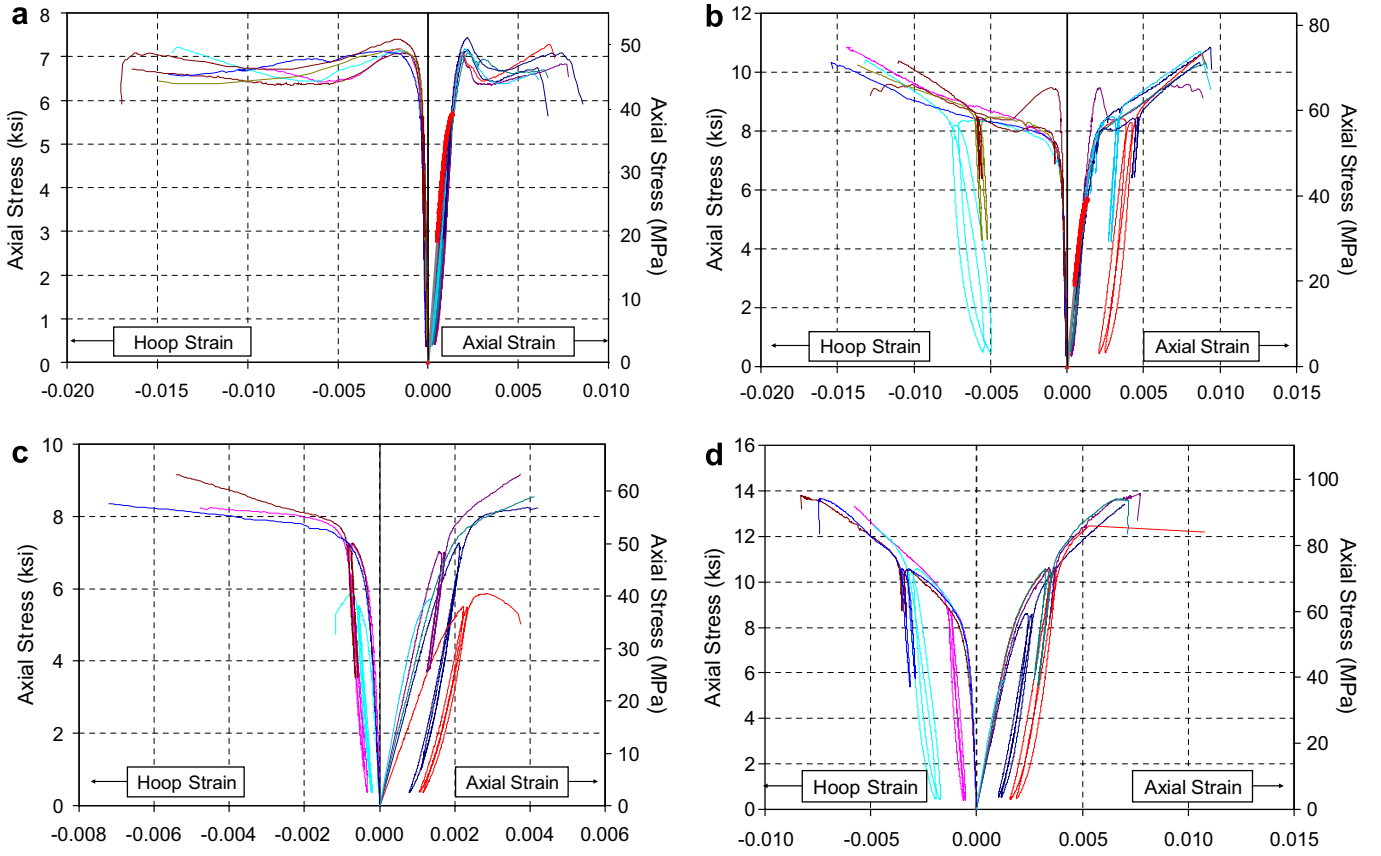

Fig. 2. Stress–strain response for FRP-confined concrete stub specimens: (a) single layer glass wraps; (b) two-layer glass wraps; (c) single layer carbon wraps; (d) two-layer carbon wraps.

Since confinement of FRP is activated by lateral expansion of concrete, it is interesting to note the effect of cyclic loading on volumetric strain ε_v of concrete, as given by

$$\varepsilon_v = \varepsilon_c + 2\varepsilon_r \tag{3}$$

where ε_c and ε_r are the axial and lateral strains, respectively. Fig. 4 shows the axial stress versus volumetric strains for two of the stubs, G22 and C25, under two different loading patterns. Positive and negative strains indicate volume contraction and expansion, respectively. In both specimens, concrete is initially contracting until about 70% of its unconfined strength. Afterwards, the wrap actively controls dilation tendency of concrete, which otherwise rapidly expands to failure. Thicker wraps can even reverse the dilation process, and lead to failure in contraction [14]. Unloading and reloading portions of the volumetric strains are quite wider for the GFRP wraps, as compared to the CFRP wraps. In neither case, however, the unloading and reloading curves follow the initial contraction rate of concrete.

3. Cyclic model

Test results from present study as well as those from [11,12] shown in Table 3 were used to develop a cyclic model for FRP-confined concrete. Test results from [13] were used for validation of the model. In this section, the envelope curve is reviewed first. Then, the rules for unloading and reloading between the envelope curve and a zero stress level are described. Finally, more generalized rules of unloading and reloading between any two arbitrary stress levels are presented.

3.1. Model for envelope curve

Results of cyclic tests, as shown in Figs. 2 and 3, indicate a unique envelope curve for FRP-confined concrete. The constitutive model of [2] for monotonic loading is chosen as the envelope curve for cyclic loading. The model has been compared and verified through several independent studies as a simple, yet accurate, description of the entire stress–strain response of FRP-confined concrete [6,7].

Fig. 5 shows the bilinear stress–strain model of [2]. The initial slope is controlled by the modulus of elasticity of concrete core, as the lateral expansion of concrete is generally limited in this region. The second slope is controlled by the hoop stiffness of the FRP jacket, as concrete core has significantly cracked and the confining action of the jacket has been activated in this region. There is a curved transition zone in between the two regions. The entire stress–strain (f_c–ε_c) response is defined as

$$f_c = \frac{(E_1 - E_2)\varepsilon_c}{\left[1 + \left(\frac{(E_1 - E_2)\varepsilon_c}{f_0}\right)^n\right]^{1/n}} + E_2\varepsilon_c \tag{4}$$

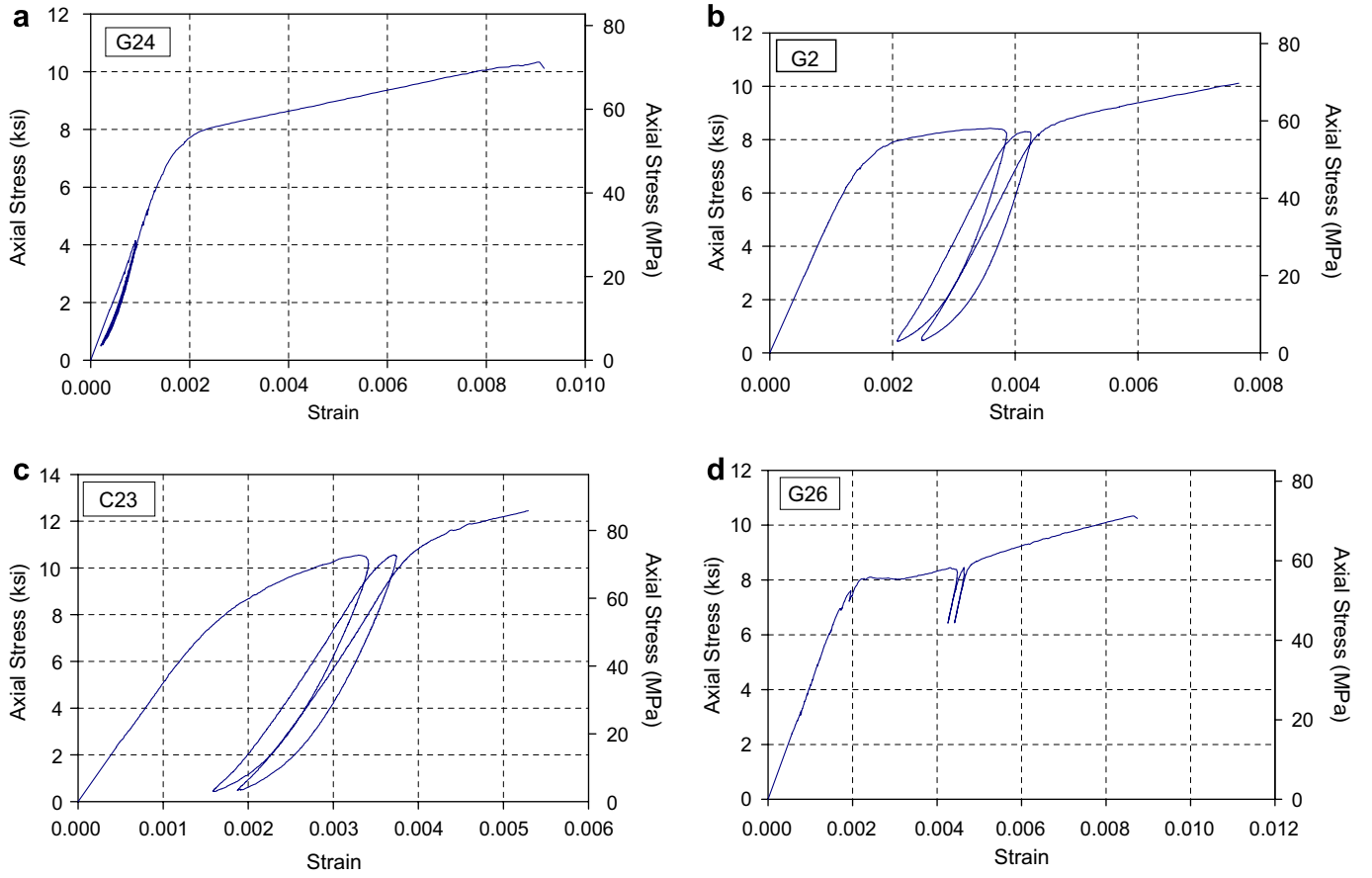

Fig. 3. Typical unloading and reloading curves: (a) typical unloading curves before bend point; (b) typical unloading curves after bend point; (c) typical reloading curves from low stress levels; (d) typical reloading curves from high stress levels.

where E_1 and E_2 are the first and second slopes of the response, respectively, given by

$$E_1 = 3950\sqrt{f'_{co}}\ \text{[MPa]} \tag{5}$$

$$E_2 = 245.61 f'^{0.2}_{co} + 1.3456\frac{E_j t_j}{D}\ \text{[MPa]} \tag{6}$$

where E_j is modulus of elasticity of FRP, and f_0 is the Y-intercept of the second slope, given by

$$f_0 = 0.872 f'_{co} + 0.371 f_r + 6.258\ \text{[MPa]} \tag{7}$$

and n is the curve shape parameter for the transition zone, selected as 1.5. The ultimate strength of FRP-confined concrete is given by

$$f'_{cu} = f'_{co} + 6.0 f'^{0.7}_{r}\ \text{[MPa]} \tag{8}$$

and finally, the ultimate strain of FRP-confined concrete can be calculated as

$$\varepsilon_{cu} = \frac{f'_{cu} - f_0}{E_2} \tag{9}$$

3.2. Unloading from envelop curve to zero stress

A total of 10 data sets were compiled from present study and two other references [11,12], for full unloading from the envelop curve to a zero stress level. As discussed earlier for Fig. 3, the unloading curve depends on the unloading stress level f_{un} and its relative location with respect to the bend point on the envelope curve. The path is linear, when unloading before the bend point on the envelope curve. On the other hand, the path is curvilinear when unloading above the bend point. Furthermore, the unloading branch below the bend point returns to the origin, whereas the unloading branch above the bend point terminates at a residual or plastic strain ε_{pl}. Test results indicate that the higher the unloading stress is, the larger the plastic strain would be. The unloading branch is therefore modeled by its secant modulus of elasticity $E_{Sec\,u}$ as

$$E_{Secu} = \frac{f_{un}}{\varepsilon_{un} - \varepsilon_{pl}} \tag{10}$$

where ε_{un} is the unloading strain on the envelope curve. Fig. 6a shows a schematic illustration of the unloading rule. Regression analysis showed a strong correlation between E_{Secu} and f_{un}. Fig. 7 shows the normalized unloading modulus E_{Secu}/E_1 versus the normalized unloading stress f_{un}/f'_{co} for all of the 10 unloading sets in the database. The range of f_{un}/f'_{co} in the database varied between 1.3 and 2.2. Based on these observations of the unloading

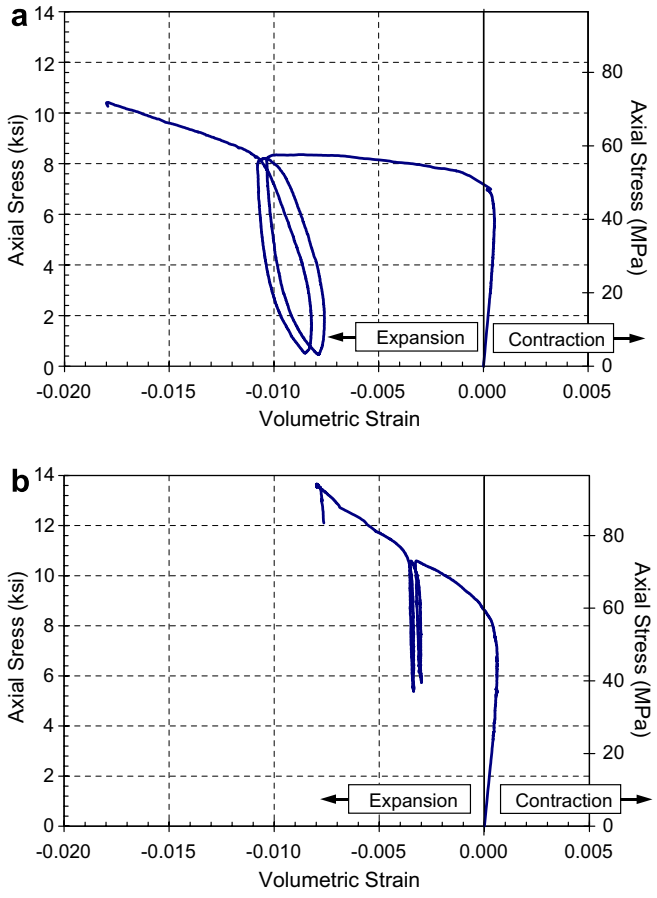

Fig. 4. Axial stress versus volumetric strain for typical specimens: (a) specimen G24; (b) specimen C25.

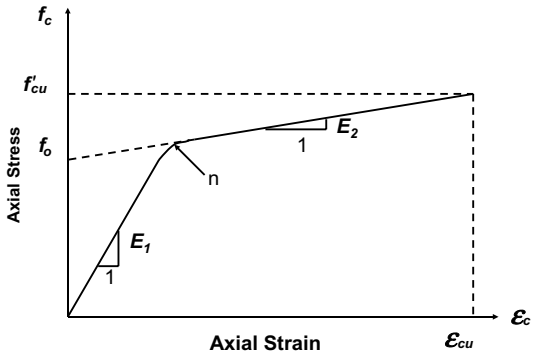

Fig. 5. Parameters of envelope curve for FRP-confined concrete from [2].

phenomenon, the following tri-linear model is proposed for $E_{\mathrm{Sec}u}$ with a 70.3% goodness of the fit:

$$\frac{E_{\mathrm{Sec}u}}{E_1} = \begin{cases} 1, & 0 \leqslant \frac{f_{\mathrm{un}}}{f'_{\mathrm{co}}} < 1 \\ -0.44 \cdot \frac{f_{\mathrm{un}}}{f'_{\mathrm{co}}} + 1.44, & 1 \leqslant \frac{f_{\mathrm{un}}}{f'_{\mathrm{co}}} < 2.5 \\ 0.34, & \frac{f_{\mathrm{un}}}{f'_{\mathrm{co}}} \geqslant 2.5 \end{cases} \tag{11}$$

Fig. 8 shows a comparison of the predicted and the experimental values for the unloading slopes. A maximum error of ±15% is noted. From Eqs. (10) and (11), for each unloading stress on the envelope curve, there is a unique $E_{\mathrm{Sec}u}$ and a unique plastic strain $\varepsilon_{\mathrm{pl}}$, as

$$\varepsilon_{\mathrm{pl}} = \varepsilon_{\mathrm{un}} - \frac{f_{\mathrm{un}}}{E_{\mathrm{Sec}u}} \tag{12}$$

It should be noted that the plastic strain can be regarded as the intersection of the unloading slope from the envelope curve to the focal or pivot point used by some hysteretic models for unconfined concrete or steel-confined concrete [10]. The unloading curve starts from the unloading point $(\varepsilon_{\mathrm{un}}, f_{\mathrm{un}})$ to the point of plastic strain $(\varepsilon_{\mathrm{pl}}, 0)$. It can also be shown that the tangent slope of the unloading branch at the point of plastic strain is almost zero. Moreover, unloading branches may be represented by a polynomial curve, such as

$$f_{\mathrm{c}} = \frac{(1-x)^{n_1}}{(1+kx)^{n_2}} f_{\mathrm{un}} \tag{13}$$

where x is the normalized strain on the unloading branch, as given by

$$x = \frac{\varepsilon_{\mathrm{c}} - \varepsilon_{\mathrm{un}}}{\varepsilon_{\mathrm{pl}} - \varepsilon_{\mathrm{un}}}, \quad 0 < x < 1 \tag{14}$$

and n_1, n_2 and k are shape parameters. Three boundary conditions are known, as follows:

1. on the envelope curve, $x = 0$, $\varepsilon_{\mathrm{c}} = \varepsilon_{\mathrm{un}}$, and $f_{\mathrm{c}} = f_{\mathrm{un}}$;
2. at the zero stress level, $x = 1$, $\varepsilon_{\mathrm{c}} = \varepsilon_{\mathrm{pl}}$, and $f_{\mathrm{c}} = 0$; and
3. the tangent slope of the unloading branch at any point is given by

$$\frac{\partial f_{\mathrm{c}}}{\partial \varepsilon_{\mathrm{c}}} = \frac{n_1(1-x)^{n_1-1}(1+kx)^{n_2} + n_2(1-x)^{n_1}k(1+kx)^{n_2-1}}{(1+kx)^{2n_2}} E_{\mathrm{Sec}u} \tag{15}$$

and its value on the envelope curve ($x = 0$) is given by

$$E_u = (n_1 + n_2 k) \cdot E_{\mathrm{Sec}u} \tag{16}$$

and at the point of plastic strain ($x = 1$), the slope is 0, as expected.

Fig. 9 shows the normalized stress–strain data from unloading test data in the database. Regression analysis from all data sets found all shape parameters to be equal to 2, simplifying the unloading branch as

$$f_{\mathrm{c}} = \frac{(1-x)^2}{(1+2x)^2} f_{\mathrm{un}} \tag{17}$$

Therefore, the tangent slope of the unloading branch on the envelope curve turns out to be six times the secant unloading slope $E_{\mathrm{Sec}u}$.

3.3. Reloading from zero stress to envelope curve

Although some softening can be seen at the onset of reloading, it is typically modeled as a linear curve. Reload-

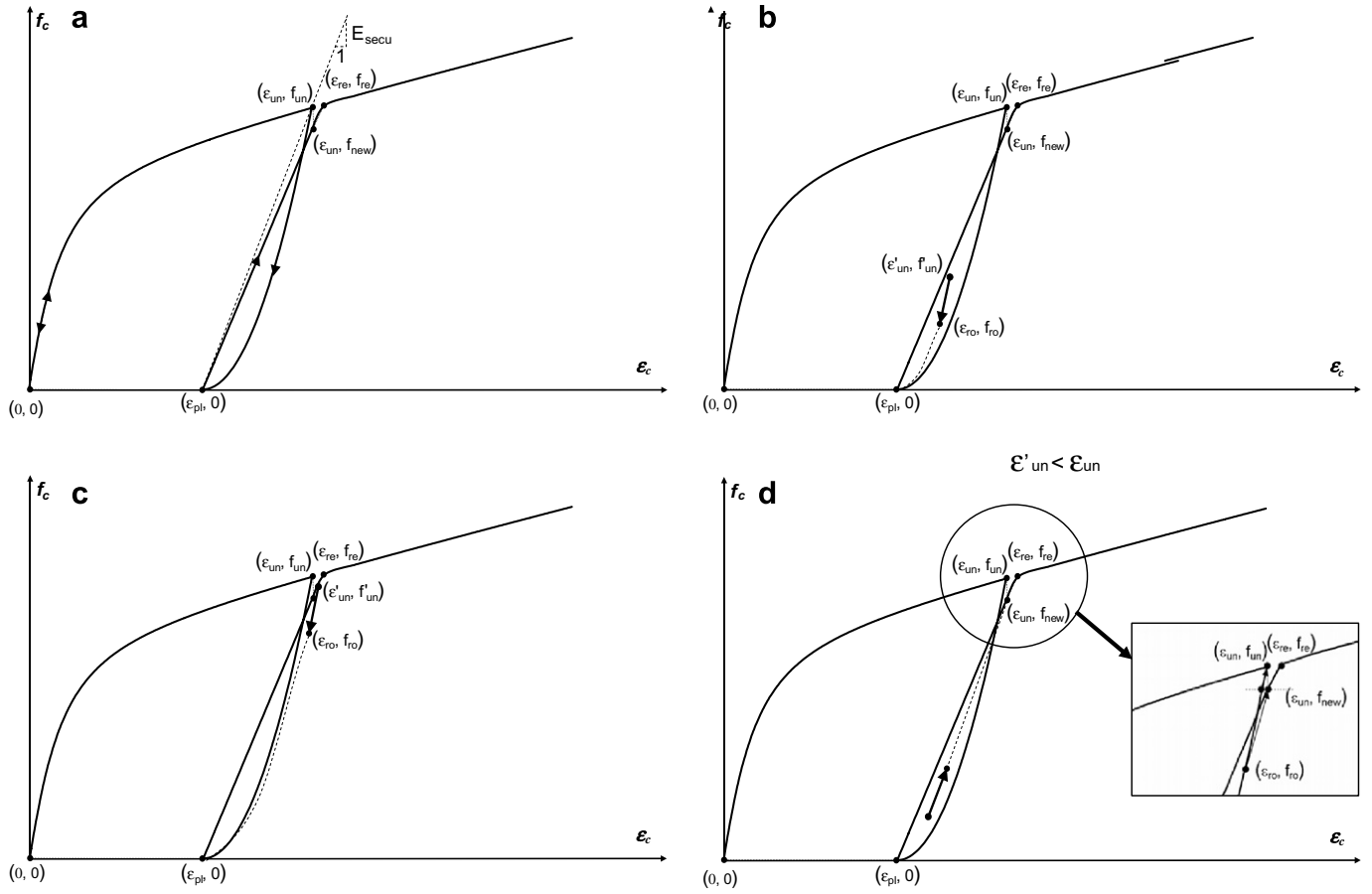

Fig. 6. Rules of the proposed cyclic model: (a) unloading and reloading between envelope curve and zero stress; (b) unloading from an arbitrary stress level $\varepsilon'_{un} < \varepsilon_{un}$; (c) unloading from an arbitrary stress level $\varepsilon'_{un} > \varepsilon_{un}$; (d) reloading from an arbitrary stress level.

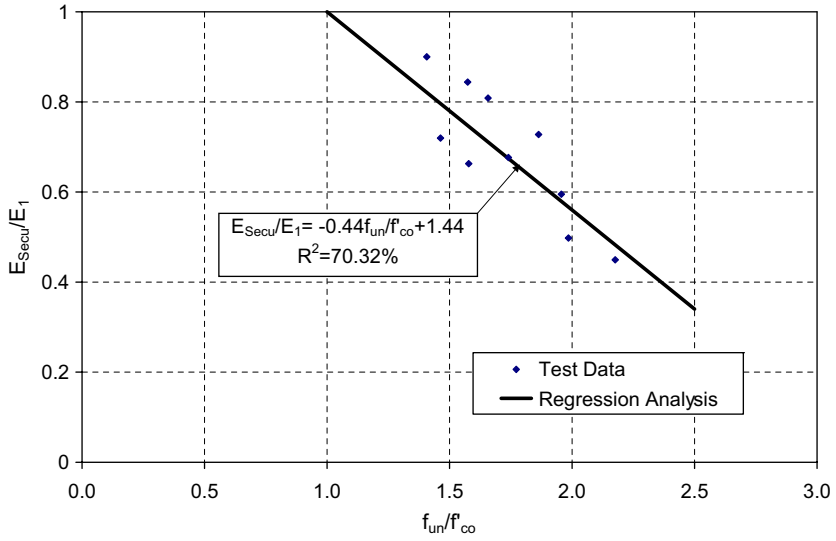

Fig. 7. Regression analysis of unloading slopes.

ing back to the envelope curve on the initial slope constitutes no stiffness or strength degradation. Above the bend point, however, strength and stiffness degradations are prevalent due to internal cracks. Concrete does not return to the unloading stress f_{un} at the unloading strain ε_{un}, but rather a lower stress of f_{new}. Fig. 10 shows a 10% strength degradation for the 22 reloading data sets with a 90% goodness of the fit. The new stress level is given by

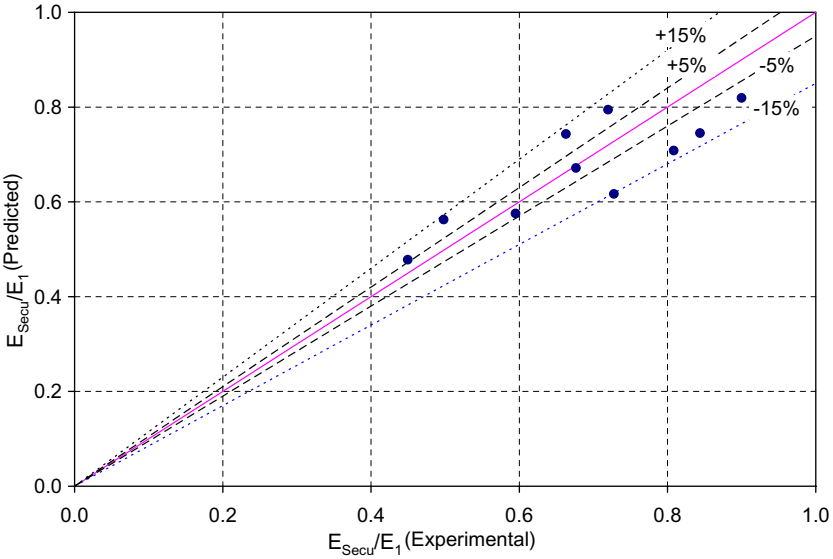

Fig. 8. Comparison of predicted and experimental values of unloading slope.

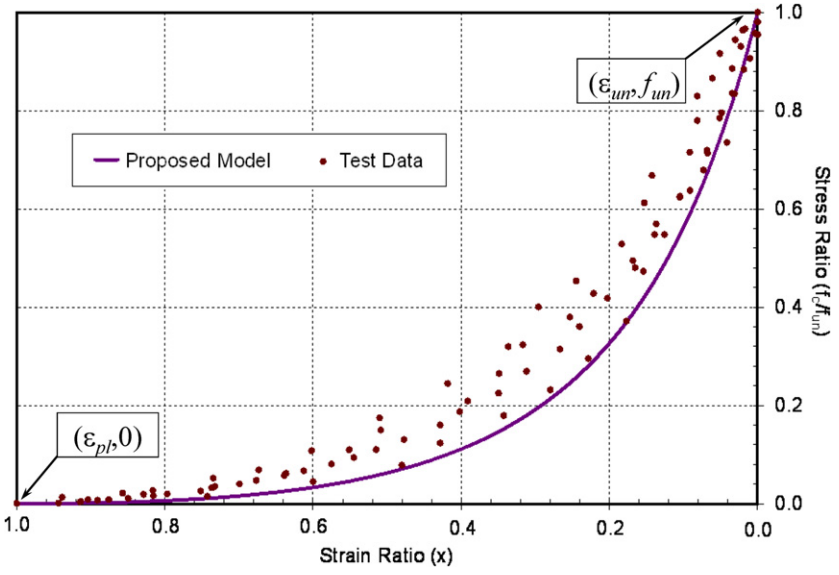

Fig. 9. Normalized unloading curves.

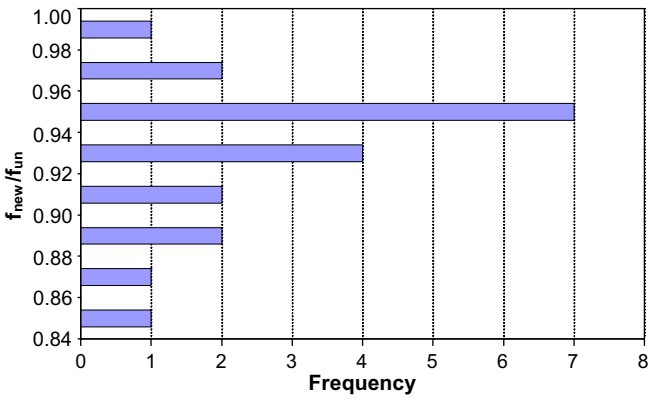

Fig. 10. Frequency distribution of strength degradation data.

$$f_{new} = 0.9 f_{un} \tag{18}$$

The reloading branch can therefore be constructed between the point of plastic strain $(\varepsilon_{pl}, 0)$ and the new stress level $(\varepsilon_{un}, f_{new})$. For simplicity, the reloading branch is then extended using the same slope until its return to the envelope curve $(\varepsilon_{re}, f_{re})$ as

$$\frac{f_{re}}{\varepsilon_{re}} = \frac{f_{new}}{\varepsilon_{un} - \varepsilon_{pl}} \tag{19}$$

where the return point $(\varepsilon_{re}, f_{re})$ can be computed in combination with Eq. (4) for the envelope curve. Fig. 6a shows the schematic illustration of the reloading rule. Due to the uniqueness of the plastic strain for each unloading point on the envelope curve, the unloading point $(\varepsilon_{un}, f_{un})$,

new stress point (ε_{un},f_{new}), and the point of plastic strain (ε_{pl}, 0) are kept constant in the hysteretic response, until a new unloading branch initiates from the envelope curve.

3.4. Unloading between arbitrary stress levels

Once E_{Secu} and ε_{pl} are determined for an unloading point on the envelope curve, the hysteretic response can be easily generalized. Unloading from any arbitrary point (ε'_{un},f'_{un}) to an eventual reloading point (ε_{ro},f_{ro}) follows a path similar to the primary unloading branch, as

$$x = \frac{\varepsilon_c - \varepsilon'_{un}}{\varepsilon_{pl} - \varepsilon'_{un}} \tag{20}$$

$$f_c = \frac{(1-x)^2}{(1+2x)^2} f'_{un} \tag{21}$$

Fig. 6b and c shows the schematic illustration of these unloading rules for the conditions of $\varepsilon'_{un} < \varepsilon_{un}$ and $\varepsilon'_{un} > \varepsilon_{un}$, respectively.

3.5. Reloading between arbitrary stress levels

Four different cases may arise during an arbitrary reloading:

1. When the reloading stress f_{ro} and the target stress f'_{un} are both less than the new stress level f_{new}, the reloading branch will follow a straight line targeting the new stress point (ε_{un},f_{new}) until it reaches f'_{un}.
2. When the reloading stress f_{ro} is lower than the new stress level f_{new}, but the target stress f'_{un} is higher than f_{new}, the reloading branch will first follow a straight line to the new stress point (ε_{un},f_{new}), and then follows the slope from the point of plastic strain (ε_{pl}, 0) to the new stress point (ε_{un},f_{new}) until it reaches the target stress.
3. When the reloading stress f_{ro} and the target stress f'_{un} are both higher than the new stress f_{new}, the reloading branch will follow the slope from the point of plastic strain (ε_{pl}, 0) to the new stress point (ε_{un},f_{new}) until it reaches the target stress of f'_{un}, where $f'_{un} \leqslant f_{re}$.
4. A subset of Case 3 above occurs when the reloading stress f_{ro} is higher than the new stress f_{new}, but the reloading strain ε_{ro} is lower than ε_{un}. In this case, the reloading branch will follow a straight line to the unloading point (ε_{un},f_{un}) until it reaches the target stress level of f'_{un}, where $f'_{un} \leqslant f_{un}$. The difference between f_{ro} and f_{un} is considered very small, and therefore, the path targets the previous unloading point (ε_{un},f_{un}) on the envelope curve rather than the return point (ε_{re},f_{re}).

Fig. 6d shows the schematic illustration of these reloading rules.

4. Verification of the cyclic model

Test data from an independent experimental study, which was excluded from the model calibration, was used to verify the proposed cyclic model of FRP-confined concrete. Chen [13] tested four concrete stubs in uniaxial compression with loading and unloading at different levels. The specimens had a 152 mm diameter and a 305 mm height. The 28-day compressive strength of concrete was 39.6 MPa. Half of the specimens were wrapped with two layers of carbon, while the other half were wrapped with three layers. The wrap was FTS-C1-30 carbon fabric from Tonen Corp. of Japan with a 0.17 mm thickness per layer, a tensile strength of 3550 MPa, a tensile modulus of 235 GPa, and an ultimate elongation of 1.5%. An epoxy resin with a tensile strength of 25 MPa was used as adhesive. The actual thickness per layer of the cured wrap varied between 0.6 and 1.0 mm. Figs. 11 and 12 show the comparison of the test results (dashed lines) and the predictions from the proposed cyclic model (solid lines) under different loading patterns for the two and three layer carbon wraps, respectively. A very good agreement is noted for all loading cases and jacket thickness.

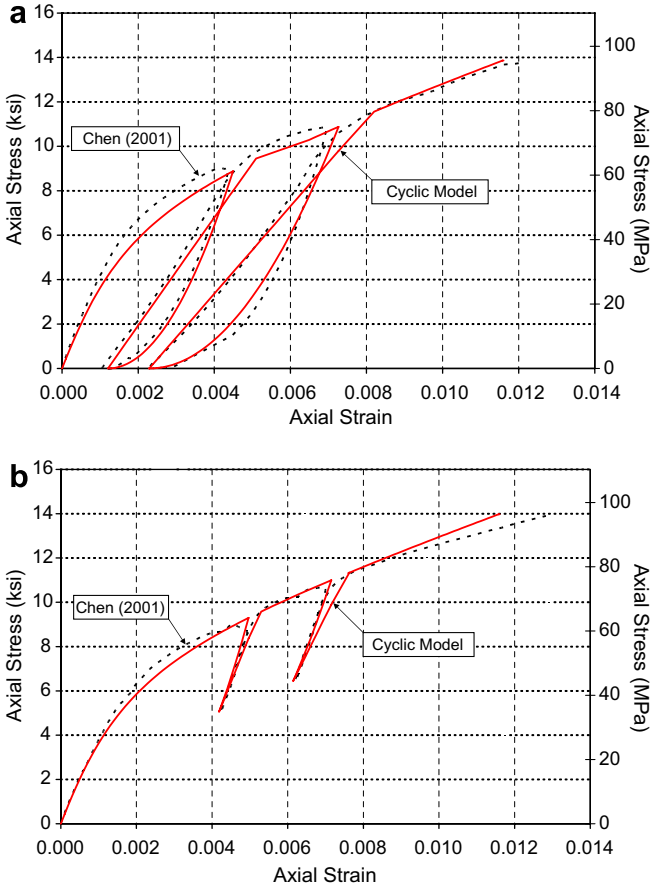

Fig. 11. Comparison of proposed model with two-layer CFRP stub specimen: (a) unloaded to zero stress; (b) unloaded to non-zero stress.

5. Conclusions

A total of 24 FRP-confined concrete stub specimens were tested in uniaxial compression under different levels of loading and unloading. Test parameters included fiber

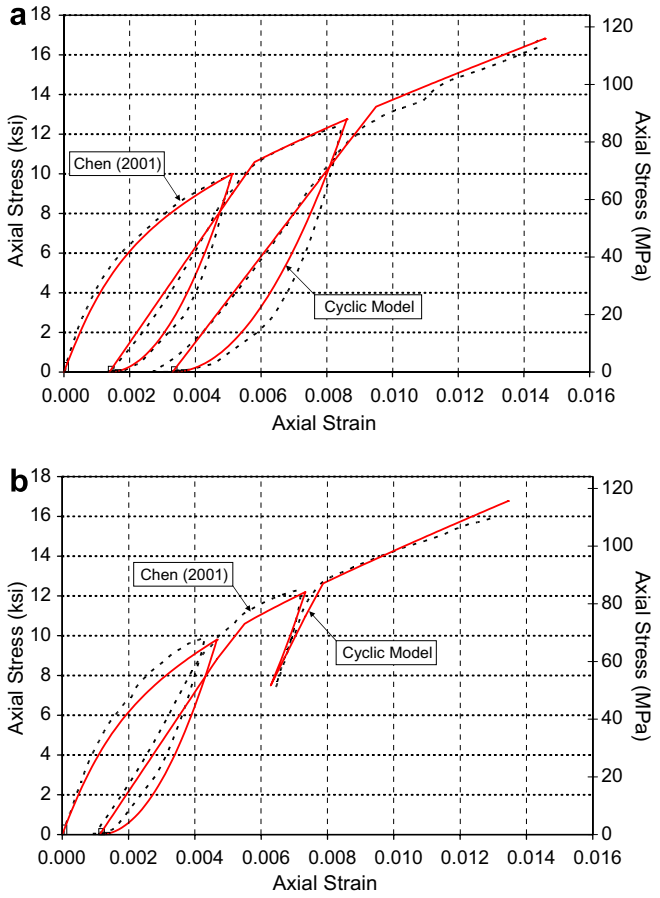

Fig. 12. Comparison of proposed model with three-layer CFRP stub specimen: (a) unloaded to zero stress; (b) unloaded to zero and non-zero stress.

type, thickness of the wrap, and loading patterns. A new model for FRP-confined concrete under uniaxial cyclic compression was proposed using regression analysis of test results. An existing bi-linear confinement model under uniaxial monotonic loading was employed to serve as the unique envelope curve. The proposed model includes cyclic rules for loading and unloading, plastic strains, and stiffness and strength degradations. Good agreement was obtained between the analytical predictions of the model with the experimental results of an independent test series, confirming the ability of the model to predict the cyclic behavior of FRP-confined concrete.

Acknowledgements

This study was sponsored by the National Science Foundation and the Florida Department of Transportation. Additional support in the form of materials was provided by Sika Corp. The views and findings reported here are those of the authors alone, and not necessarily those of the sponsoring agencies.

References

[1] Loud S. California prepares for the "Big One" with composite retrofitting. Compos Technol 1995;1(4):32–5.
[2] Samaan M, Mirmiran A, Shahawy M. Modeling of concrete confined by fiber composites. J Struct Eng – ASCE 1998;124(9):1025–31.
[3] Toutanji H. Stress–strain characteristics of concrete columns externally confined with advanced fiber composite sheets. ACI Mater J 1999;96(3):397–404.
[4] Fam AZ, Rizkalla SH. Confinement model for axially loaded concrete confined by FRP tubes. ACI Struct J 2001;98(4):451–61.
[5] Matthys S, Taerwe L, Audenaert K. Tests on axially loaded concrete columns confined by fiber reinforced polymer sheet wrapping. In: Dolan C, Rizkalla SH, Nanni A, editors. Fourth international symposium on fiber reinforced polymer reinforcement for reinforced concrete structures, SP-188, ACI; 1999. p. 243–53.
[6] De Lorenzis L. A comparative study of models on confinement of concrete cylinders with FRP composites. Technical report, Chalmers University of Technology, Goteborg, Sweden, 2001, 01:04(46).
[7] Lam L, Teng J. Strength models for fiber-reinforced plastic confined concrete. J Struct Eng – ASCE 2002;128(5):612–23.
[8] Park R, Kent DC, Sampson RA. Reinforced concrete members with cyclic loading. J Struct Eng – ASCE 1972;98(7):1341–59.
[9] Yankelevsky D, Reinhardt H. Model for cyclic compressive behavior of concrete. J Struct Eng – ASCE 1987;113(2):228–40.
[10] Mander J, Priestly M, Park R. Theoretical stress–strain model for confined concrete. J Struct Eng – ASCE 1988;117(8):1804–26.
[11] Scherer M. Design optimization and behavior of concrete-filled FRP tubes, MS Thesis, University of Central Florida, Orlando, FL, 1996.
[12] Mastrapa JC. Effect of construction bond on confinement with fiber composites, MS Thesis, University of Central Florida, Orlando, FL, 1997.
[13] Chen X, FRP-wrapped concrete short column under uniaxial compression, Final report, National Diagnosis and Rehabilitation of Industrial Building Research Center, Beijing, China, 2001.
[14] Mirmiran A, Shahawy M. Behavior of concrete columns confined by fiber composites. J Struct Eng – ASCE 1997;123(5):583–90.